A VORTICITY STRETCHING DIAGNOSTIC FOR TURBULENT FLOWS

Johan Malm[1,*], **Philipp Schlatter**[1], **Neil D. Sandham**[2]

[1]Linné FLOW Centre, SeRC, KTH Mechanics, SE-100 44, Stockholm, Sweden

[2]School of Engineering Sciences, University of Southampton, Southampton, SO17 1BJ, UK

ABSTRACT

Vorticity stretching in wall-bounded turbulent and transitional flows has been investigated by means of a new diagnostic, designed to pick up regions with large amounts of vorticity stretching. It was found that the largest occurrence of vorticity stretching in fully turbulent channel flows is present at a wall-normal distance of $y^+ = 6.5$, *i.e.* in the transition between the viscous sublayer and the buffer region. Instantaneous data showed that the coherent structures associated with these stretching events have the shape of flat 'pancake structures' in the vicinity of high-speed streaks, here denoted 'h-type' events. The other event found, also studied in an asymptotic suction boundary layer, is the 'l-type' event present on top of an unstable low-speed streak. These events are further thought to be associated with the exponential growth of streamwise vorticity in the turbulent near-wall cycle.

INTRODUCTION

In wall-bounded turbulent flows, streamwise velocity streaks (Kline *et al.*, 1967) and quasi-streamwise vortices (Smith & Metzler, 1983) are known to dominate the near-wall region. Hamilton *et al.* (1995); Jiménez & Pinelli (1999) and others showed that these structures are tied together via a self-sustained cycle, where the streamwise vortices create streaks and the streaks break down to create new streamwise vortices. Minimal flow units (Jiménez & Moin, 1991) were used to show that if this cycle was broken at any point the flow would relaminarise. While the mechanism in which streaks are created by streamwise vortices is fully understood and well documented (*e.g.* Klebanoff *et al.*, 1962; Landahl, 1980), there has been less consensus on how the streaks break down and the streamwise vortices are recreated. There are however indications (*e.g.* Waleffe, 1997) that the breakdown is preceded by exponential growth of x-dependent disturbances. For the late stages of the streak instability phase, Schoppa & Hussain (2002) elaborated on a mechanism responsible for the formation of streamwise vortex sheets which eventually collapse due to the stretching caused by the streamwise strain, $\partial u/\partial x$. This shows that vorticity stretching may be an important ingredient in the near-wall cycle. There is also some evidence (Jones *et al.*, 2009) that vorticity stretching plays an important role in self-sustained transition processes, such as the unsteady vortex shedding in a separated flow. In addition, during the end-stage of K-type transition, it has been noted (Sandham & Kleiser, 1992) that the stretching of vorticity involved in the roll-up of detached shear layers leads to turbulence regeneration. The fact that the vorticity stretching itself provides a rapid growth mechanism becomes evident when studying the vorticity transport equation in an incompressible flow. Assume there is initially some vorticity, ω_s, and strain, $\partial u_s/\partial s$, in the direction of s, where s is the strain elongation axis. Assume further that the strain is negligible in the other spatial directions so that the vorticity tilting terms vanish; then the vorticity transport equation reduces to $\frac{D\omega_s}{Dt} = \omega_s \frac{\partial u_s}{\partial s}$, provided the Re is high enough so that the damping term $\nu\nabla^2\omega_s$ is small. Solving for ω_s gives $\omega_s \sim \exp\left(\frac{\partial u_s}{\partial s} t\right)$, *i.e.* exponential growth of vorticity along s, assuming a constant strain rate following the fluid element. The above mentioned examples indicate that vorticity stretching is dynamically important for the growth of instabilities in wall-bounded flows. Therefore, we intend to study this mechanism in more detail in three different flows with successively increasing complexity: A near-wall cycle in an asymptotic suction boundary layer; K-type transition in a plane channel flow and fully turbulent channel flow. As we progress towards fully turbulent, spatially unconstrained flows the increased complexity needs to be handled accordingly and we need tools to extract the flow physics. In order to locate the largest occurrence of vorticity stretching in the flow, we will define the following scalar measure:

$$\Gamma_p(x,y,z,t) = \max\{\alpha|\omega_\alpha|, \beta|\omega_\beta|, \gamma|\omega_\gamma|\}, \tag{1}$$

where α, β and γ are the eigenvalues of the strain tensor $S_{ij} = \frac{1}{2}(\frac{\partial u_i}{\partial u_j} + \frac{\partial u_j}{\partial u_i})$ and ω_α, ω_β and ω_γ are the vorticity components along the principal axes given by the eigenvectors of S_{ij}. The subscript 'p' indicates that we are in a principal axis system, aligned with the direction of strain. The procedure of decomposing the strain tensor into its eigenvectors is commonly adopted in studies of homogeneous turbulence where the usual spatial coordinate directions have a subordinated meaning, (*e.g.* She *et al.*, 1991; Nomura & Post, 1998). We will compare this measure to the following:

$$\Gamma_c(x,y,z,t) = \max\{|\omega_x|\frac{\partial u}{\partial x}, |\omega_y|\frac{\partial v}{\partial y}, |\omega_z|\frac{\partial w}{\partial z}\}, \tag{2}$$

where the subscript 'c' denotes 'Cartesian'. The region of intense Γ will further be linked to the birth of vortices by lo-

*johan@mech.kth.se

cating high concentration of λ_2 (Jeong & Hussain, 1995) in the flow.

NUMERICAL METHOD & SIMULATION SETUP

The solutions of the incompressible Navier–Stokes equations were obtained by a Chebyshev-Fourier pseudo-spectral code described in Chevalier *et al.* (2007). Each one of the three cases are described more in detail below.

Near-wall cycle in an asymptotic suction boundary layer (sinuous instability)

The asymptotic suction boundary layer (ASBL) enables the study of an open boundary layer in the temporal framework, *i.e.* by employing suction at the wall the spatial growth of the boundary layer is removed, which opens the possibility of using a streamwise periodic domain. Hence, for the present simulation, employed at a Reynolds number of $Re = U_\infty \delta^*/\nu = U_\infty/V_\infty = 750$ (U_∞ being the free-stream velocity, δ^* the displacement thickness and V_∞ the imposed vertical velocity) we used a computational domain with periodic boundary conditions in the spanwise and streamwise directions. A Dirichlet condition in the form of a constant velocity (V_∞) in the negative vertical direction was applied at the bottom of the domain. The dimensions of the domain (non-dimensionalised by δ^*) were chosen as $L_x = 12$, $L_y = 15$ and $L_z = 6$, such that the flow would be a 'minimal flow unit' and the dynamics of a single streak could be studied. A satisfactory spatial resolution was chosen to be $N_x = 32$, $N_z = 32$ Fourier modes in the streamwise and spanwise directions and $N_y = 129$ Chebyshev modes in the wall-normal direction. The critical trajectory ('edge state') was found by bisection where the amplitude of the random initial condition was tuned such that the flow neither becomes turbulent nor goes laminar (Schneider *et al.*, 2007). The result is a time-periodic orbit with a period of $T = 3347$. The edge state in the ASBL flow was computed and studied by Madré (2011) and discussed by B. Eckhardt (ETC-12, 2009, Marburg). The aim of the present case is however not to study its state-space properties, but merely to use the case as an alternative to minimal channel flows in an effort to simplify turbulent dynamics as much as possible. Some snapshots representative for the streak instability phase, breakdown and streak regeneration are shown in Figure 1. The initially straight low-speed streak at $t = t_0$ (Figure 1*a*) is indicated by the gray surface of constant streamwise velocity. Soon, around $t = t_0 + 0.16T$, the low-speed streak experiences a sinuous instability and x-dependent disturbances are amplified (Figure 1*b*). As the disturbance growth has reached nonlinear amplitudes ($t = t_0 + 0.39T$, Figure 1*c*) the streak breaks down into smaller scales. During this phase, streamwise vortices are regenerated which leads to the growth of a new streak, displaced $L_z/2$ to the left. Thus, the flow at $t = t_0 + 0.5T$ shown in Figure 1(*d*), is the exact symmetric equivalent to the flow in Figure 1(*a*) with respect to a spanwise midplane.

Subcritical K-type transition (varicose instability)

Direct numerical simulation (DNS) of subcritical K-type transition at Re_b = 3333 were performed in order to examine the role of vorticity stretching in a classical transitional

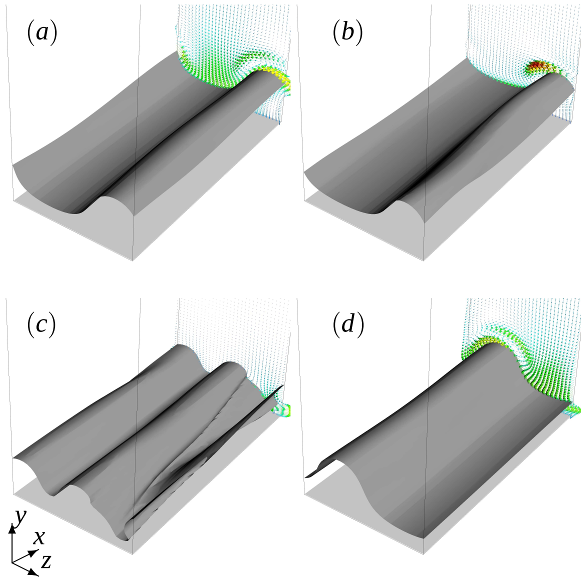

Figure 1. Evolution of the low-speed streak indicated by a surface of constant streamwise velocity, $u = 0.6$ (*gray*), at (*a*) $t = t_0$, (*b*) $t = t_0 + 0.16T$, (*c*) $t = t_0 + 0.39T$ and (*d*) $t = t_0 + 0.5T$, where T denotes the period of the periodic orbit. Vectors of crossflow velocities are shown in a crossflow plane.

flow (Gilbert & Kleiser, 1990). The initial disturbances consist of a two-dimensional TS wave with a streamwise wave number of α = 1.12 and an amplitude of 3% of the laminar centre-line velocity; together with two three-dimensional oblique waves with wave numbers α = 1.12 and β = 2.1 and amplitudes of 0.05%. This wave packet, superimposed on a laminar Poiseuille channel flow, experiences an exponential growth eventually leading to turbulent breakdown. Around $t = 120$ the Λ-vortex appears, which develops into a hairpin vortex at $t \approx 135$. Shortly thereafter ($t \approx 160$), the highly fluctuating transitional phase sets in; and finally, at $t \approx 220$, the flow has reached a fully developed turbulent state. The box lengths were $L_x \times L_y \times L_z = 2\pi/\alpha \times 2 \times 2\pi/\beta$ and the resolution used was $N_x \times N_y \times N_z = 128 \times 129 \times 128$, inspired by Gilbert & Kleiser (1990).

Turbulent channel flow at Re_τ = 180

Fully turbulent channel flow simulations were performed at a Reynolds number of Re_τ = 180, based on friction velocity, u_τ, and channel half height, h, in order to study the vorticity stretching diagnostics in a fully turbulent flow. Periodic boundary conditions in both the streamwise and spanwise directions were applied in a domain of size $L_x \times L_y \times L_z = 4\pi \times 2 \times 2\pi$ and a resolution of $N_x \times N_y \times N_z = 128 \times 129 \times 128$ (Moser *et al.*, 1999).

RESULTS

In the following, the evaluation of Γ_c and Γ_p in these three flow cases is presented.

1. The effect of sinuous instabilities on vorticity stretching

In order to facilitate understanding, Γ_c (retaining component information more obviously) is as a first step computed in the asymptotic suction boundary layer, with its evolution shown together with λ_2 in Figure 2 at similar instants as in Figure 1. As long as the high- and low-speed streaks are (reasonably) straight, most of the vorticity stretching activity resides in the high-speed streak, close to the wall (Figure 2*a*). Here, we observe that isosurfaces of constant Γ_c appear as flat 'pancake structures' close to the wall. A closer investigation reveals that $\Gamma_c = |\omega_z|\partial w/\partial z$, *i.e.* vorticity is stretched most intensively in the spanwise direction. As soon as the x-dependent disturbances are amplified and the streak starts to 'wiggle', we rather observe the highest values of Γ_c on the top of the low-speed streak (Figure 2*b*). Henceforth, we will refer to the former event as 'h-type' (high-speed) and the latter as 'l-type' (low-speed). Also here, Γ_c is in all points equal to spanwise vorticity stretching, save that the sign is different due to the absolute value in the Γ_c-measure. As for the high-speed streak, the appearance of vorticity stretching alternates from side to side also on the low-speed streak, such that the highest values are always found on the convex side of the streak. The reason for this can be understood by studying the sketch in Figure 3. Due to the mean shear, there are always high values of spanwise vorticity, ω_z, present close to the wall (A). In the case of a straight streak (Figure 3*a*) this vorticity is lifted by the streamwise vortices, due to the well-known lift-up effect (Landahl, 1980). In the braid region above the streak (B) the highest values of $\partial w/\partial z$ are found,

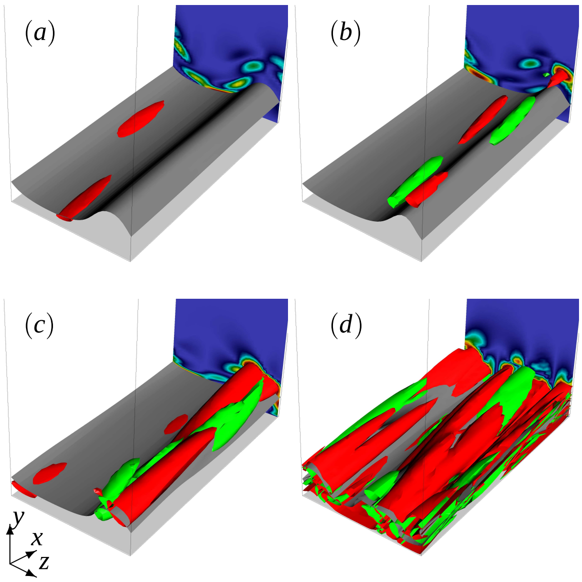

Figure 2. Evolution of Γ_c (*red*) and λ_2 (*green*) shown at (*a*) $t = t_0$, (*b*) $t = t_0 + 0.16T$, (*c*) $t = t_0 + 0.30T$ and (*d*) $t = t_0 + 0.39T$, where T denotes the period of the periodic orbit. The levels of the corresponding isosurfaces are fixed. The isosurface of streamwise velocity, $u = 0.5$ (*gray*), indicates streaks and the crossflow plane is coloured by Γ_c.

which together with the lifted vorticity creates large spanwise vorticity stretching, $\omega_z\partial w/\partial z$. A similar situation is found to be present when the streak is bent (Figure 3*b*). Since the braid region has moved over to the convex side of the streak (left in Figure 3), this is where we find high values of Γ_c. Similarly, high values of Γ_c are found to the right as soon as the streak 'wiggles' over to this side (*dashed*). It should be pointed out that the same mechanism is responsible for the high values of spanwise stretching alternating from side to side below the high-speed streak, given that the sketch in Figure 3 in that case would be upside down. The cartoon in Figure 3 is confirmed

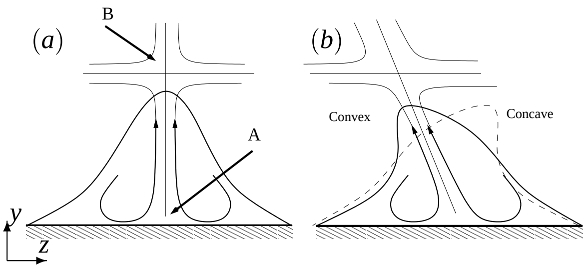

Figure 3. Explanation for an 'l-type' event: (*a*) straight streak, where high values of ω_z are lifted from A and multiplied by spanwise strain in B; (*b*) similar mechanism for a bent streak in one of its outer positions.

by results from the numerical simulation. In particular, a top view of a velocity field at $t = t_0 + 0.18T$ is provided in Figure 4(*a*), where the relation between Γ_c, Γ_p, λ_2 and the low-speed streak can be seen. It shows that high values of $\Gamma_{c,p}$ indeed are located on the convex side of the bent streak. Here, we also note that the differences between Γ_c and Γ_p are small. A more detailed comparison is given in Figure 4(*b*,*c*), where the isosurface level is decreased approximately by a factor of two. Still, Γ_c and Γ_p are located in similar regions in the flow. More specifically, they both pick up vorticity stretching on top of the low-speed streak and beneath the high-speed streak near the wall associated with the creation of drag (*i.e.* the 'pancake structures'). It is evident that, although being located in the same regions, tilted at the same angle from the wall and being similarly flat, larger pancake structures are present in the case of Γ_c as compared to Γ_p. The main difference noteworthy is that whereas Γ_c is decoupled from the quasi-streamwise vortices, Γ_p is capable of picking up the vorticity stretching associated with those, shown in Figure 4(*b*). The reason for this is thought to be the slight tilting of the vortices in the flow, such that the vorticity stretching in the streamwise direction is small. In a principal axis system, however, this tilting is accounted for.

In order to see if $\Gamma_{c,p}$ can be linked to the existence of exponential growth, we show the evolution of the vorticity components $|\omega_i|$ together with $|\lambda_2|$ and $|\Gamma_{c,p}|$ in Figure 5(*a*). More specifically, at each time the maximum absolute value over the domain, Ω, is found, *i.e.* $\max_\Omega\{|\cdot|\}$[1]. The variables are

[1] In the case of λ_2, only negative values isolate vortices (Jeong & Hussain, 1995), *i.e.* $\max_\Omega\{|\min(\lambda_2, 0)|\}$ would be the correct operation. However, we have noted that the maximum absolute value always equals the absolute value of the largest negative value, *i.e.* $\max_\Omega\{|\lambda_2|\} \equiv \max_\Omega\{|\min(\lambda_2, 0)|\}$.

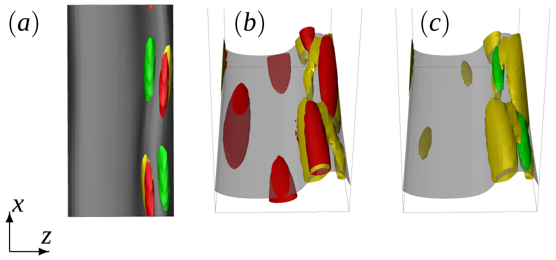

Figure 4. Isosurfaces of (*a*) $\Gamma_c = \Gamma_p = 0.0040$ (*red* and *yellow*, respectively) in a top view (aligned with the coordinate axes) and (*b*,*c*) $\Gamma_c = \Gamma_p = 0.0023$ from behind at an angle, at $t = t_0 + 0.18T$, together with $u = 0.6$ (*gray*) and λ_2 (*green*).

scaled in outer units and $t/T = 0$ corresponds to t_0 in Figure 2. Due to the mean shear, ω_z is the overall strongest vorticity

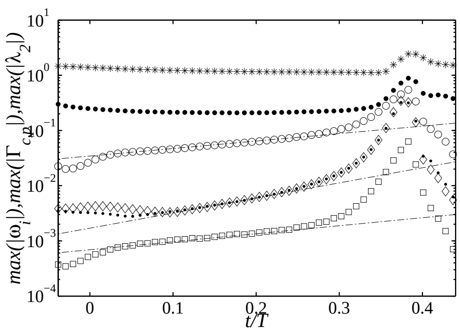

Figure 5. Maximum absolute value over Ω of ω_z ($*$), ω_y ($\bullet$), ω_x ($\circ$) together with λ_2 ($\boxdot$), Γ_c ($\diamond$), Γ_p ($\cdot$) during the streak instability phase and the nonlinear breakdown. Straight lines indicating exponential growth are included for reference. Here, $t/T = 0$ corresponds to t_0 in Figure 2.

component. The second strongest component is ω_y due to the existence of high- and low-speed streaks and the corresponding shear layer in between them. The first aspect to notice is that there is a slight decrease of these two vorticity components before the nonlinear breakdown. However, the weakest component, ω_x, is increasing. As indicated by the straight dash-dotted line the growth is weakly exponential. A similar growth rate is observed for λ_2. As $\Gamma_{c,p}$ involves the large spanwise vorticity, its growth rate is higher than the former two, albeit still exponential. Furthermore, the two measures are observed to behave very similarly. None of the ω_x-tilting terms (not shown) show any tendencies to grow exponentially.

2. The effect of varicose instabilities and the transition to turbulence on vorticity stretching

As a second step, $\Gamma_{c,p}$ is computed in K-type transition, where the initial spanwise vortex is tilted in the streamwise direction and stretched as the hairpin vortex emerges in the peak plane (Sandham & Kleiser, 1992). In Figure 6 isosurfaces of Γ_c and λ_2 are plotted shortly before (*a*) and after (*b*) the hairpin is created. Similar results are obtained for Γ_p, and

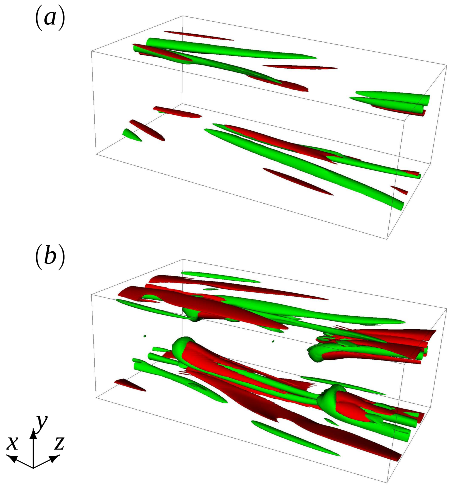

Figure 6. Isosurfaces of λ_2 (*green*) and Γ_c (*red*) during K-type transition at (*a*) an early stage ($t = 125.5$) and (*b*) at $t = 136.5$ when the hairpin vortex has emerged in the peak plane.

are thus not shown independently. In the early stage (Figure 6*a*) the Γ-measure acts as a precursor to the shear layer and the hairpin vortex formation. As for the ASBL, it also identifies the role of vorticity stretching in generating high speed streaks near the wall ('h-type'). Similarly, high values of vorticity stretching are found slightly above and in between the legs of the Λ-vortex, where the head of the hairpin vortex is about to appear ('l-type'). This mechanism is similar to the one sketched in Figure 3, due to the positive wall-normal velocity induced by the legs of the Λ-vortex. In Figure 6(*b*) we note that the Γ-measure is properly aligned with the hairpin vortex. As for the previous flow case, we include the evolution of the maximum absolute values in Figure 7 for a more quantitative comparison. Again, it can be observed that the amplitude of spanwise vorticity is nearly constant, while the streamwise and wall-normal components grow exponentially. It is interesting to notice that λ_2 is constant for a long time, but starts to increase rapidly around $t = 100$. This shows that Γ is capable of predicting instabilities.

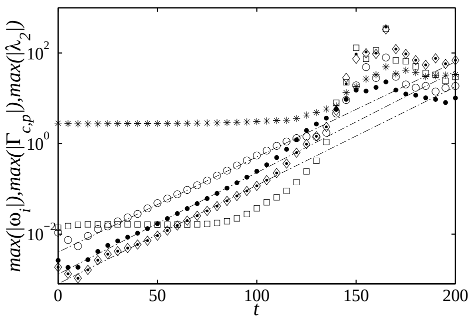

Figure 7. Maximum absolute value over Ω of ω_z ($*$), ω_y ($\bullet$), ω_x ($\circ$) together with λ_2 ($\boxdot$), Γ_c ($\diamond$), Γ_p ($\cdot$) during the streak instability phase and the nonlinear breakdown. Straight lines indicating exponential growth are included for reference. Here, $t/T = 0$ corresponds to t_0 in Figure 2.

3. Vorticity stretching in a fully turbulent flow

Next, we investigate the role of the vorticity stretching diagnostics in a fully turbulent wall-bounded flow. In particular, we are interested to see if similar events ('h' and 'l') can be observed as in the two previous flows. In Figure 8(*a*) a snapshot of a fully developed channel flow is shown (colours as before). The most prominent events are observed to be the 'pancake structures' ('h-type') adjacent to the high-speed streaks. Also a few 'l-type'-events can be found in locations of strong low-speed streak activity (indicated by the arrow). In Figure 8(*b*) we show Γ_c (*upper*), Γ_p (*lower*) together with λ_2. We note that the 'pancake structures' are essentially the same in both cases. The main difference is highlighted by the arrow in Figure 8(*b, lower*), where the structure forms a 'front' in the case of Γ_p, not present in the case of Γ_c. This difference is thought to be of the same origin as the one in Figure 4; namely that the region of intense stretching is inclined and therefore artificially cut by Γ_c but shown in its full length by Γ_p. In some locations in Figure 8(*b*) it can be seen that regions of strong vorticity stretching give rise to quasi-streamwise vortices. As soon as a vortex is created, it is convected away from the 'active' region of the flow. Many of these 'passive' vortices are seen to be located far from the wall in Figure 8(*b*), where the turbulent production is low. In that sense, the location of vorticity stretching (as opposed to vortices) pin-points the regions in a flow being dynamically relevant. Mean and

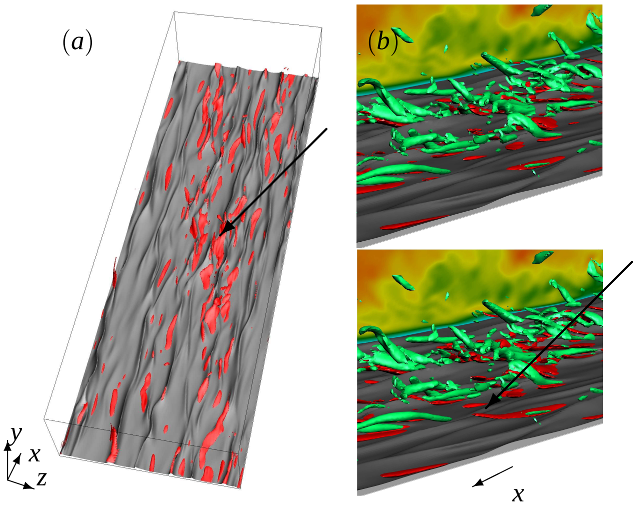

Figure 8. (*a*) Γ_c (*red*) and $u = 0.3$ (*gray*) in a fully turbulent channel flow; the arrow indicates an 'l-type'-event. (*b*) Close-up view of the same flow field, where Γ_c (*upper*) is compared to Γ_p (*lower*) and shown together with λ_2 (*green*) and a plane of streamwise velocity; the arrow shows the 'front' of the structure captured by Γ_p.

root-mean-square (r.m.s) profiles of $\Gamma_{c,p}$ and λ_2 are shown in figure 9(*a*), where the mean is taken over the homogeneous directions x, z, t. We observe the peak of both Γ-measures to be located at $y^+ = 6.5$, *i.e.* in the transition between the viscous sublayer and the buffer region. The peak of Γ_p is around 50 % higher compared to Γ_c, whereas the mean fluctuation of Γ_c show a nearly identical behaviour with that of Γ_p with maxima being located slightly closer to the wall, at $y^+ = 4.4$. The fact that the mean fluctuations peak at approximately the same wall-normal distance as the mean itself suggests that the vorticity stretching is not only a result of the mean shear but part of a dynamical process. As also noted by Jeong *et al.* (1997), since $\lambda_2 > 0$ for $y^+ \lesssim 10$, no vortices are present in the viscous sublayer. These authors further point out that the peak of λ_2' (r.m.s) at $y^+ \approx 21$ infers that the prominence of vortical structures is located in the buffer region. This indicates that, similar to the discussion above, vorticity stretching is most active in the viscous sublayer and is part of the creation of vortical structures, which are then convected outwards in the flow. In order for the vorticity to grow exponentially, there should be a predominance of stretching terms in the enstrophy transport equation (*i.e.* small amounts of tilting). Therefore, the ratio $r = \langle |\sum_\alpha \omega_\alpha^2 \frac{\partial u_\alpha}{\partial x_\alpha}|\rangle / \langle |\omega_i \omega_j \frac{\partial u_i}{\partial x_j}|\rangle$, where $\langle\cdot\rangle$ is taken over the homogeneous directions is examined. The result is thus a function of wall-normal distance, shown in Figure 9(*b*) together with the numerator and denominator separately. The ratio r can be interpreted as the enstrophy produced solely by stretching compared to the total enstrophy production (*i.e.* stretching and tilting). The horizontal line drawn at $r = 1/3$ indicates the degree of equipartition between stretching and tilting. The results suggested by Figure 9(*b*) is that the enstrophy production is dominated by stretching over tilting close to the wall, with the peak of r being attained at $y^+ \approx 3.5$. Further out in the log-region ($y^+ \approx 70$) it approaches the equipartitioned state of $1/3$. This demonstrates that the near-wall cycle contains the stretching of vorticity as an important ingredient and confirms that stretching becomes less important further away from the wall.

CONCLUSIONS

Vorticity stretching is known to provide a rapid (exponential) growth mechanism, hence the location of vorticity stretching may reveal regions of dynamical importance in the flow. Therefore, we have defined a diagnostic measure which can locate these areas. Two different variants have been investigated: One is rotationally invariant (Γ_p), and thus a true scalar quantity; the other is defined in a Cartesian framework (Γ_c), facilitating implementation and understanding. It can be concluded that the two measures do not differ from each other significantly. Generally, vorticity stretching was found to be present in conjunction with the lift-up effect creating low-speed streaks (and the equivalent effect creating high-speed streaks). In particular, in both the ASBL (acting as a model for wall-bounded turbulence) and in the fully turbulent channel flow at $Re_\tau = 180$, large amounts of vorticity stretching were found on the convex side of high-speed streaks ('h-type'-events), taking the form of large, flat 'pancake structures'. In locations of strong low-speed streak activity a similar but reversed phenomenon was observed on top of the low-speed streaks ('l-type'-events); also here on the convex side of the streak. During the streak instability phase, exponential growth of streamwise vorticity was observed in the ASBL, while the other components decayed, in line with the observations by Waleffe (1997). The rotationally invariant measure (Γ_p) could moreover detect vorticity stretching located within the core of the streamwise vortices, which gives some evidence for the mechanism suggested by Schoppa & Hussain (2002), where streamwise vortex sheets break down due to

(a)

(b)

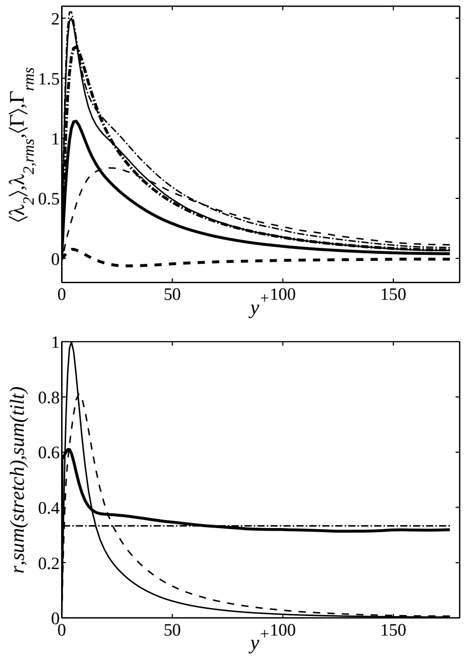

Figure 9. (*a*) Mean and r.m.s. profiles of Γ_c (——— & ———), Γ_p (—·— & —·—) and λ_2 (- - - - & - - - -); (*b*) the enstrophy production ratio, r (———) with —·— indicating $r = 1/3$, together with $\langle|\sum_\alpha \omega_\alpha^2 \frac{\partial u_\alpha}{\partial x_\alpha}|\rangle$ (———) and $\langle|\omega_i \omega_j \frac{\partial u_i}{\partial x_j}|\rangle$ (- - - -).

stretching. In K-type transition, the measures did accurately locate the regions of interest, in particular the formation of high speed streaks near the wall ('h-type') and the appearance of the hairpin vortex ('l-type'). Here, the vorticity stretching diagnostics were noticed to appear and grow long before the vortices (λ_2) showed any tendencies to grow. Shortly before the turbulent breakdown the growth of λ_2 rapidly overtook the growth of any other quantity, which shows that Γ is capable of predicting growing instabilities. Statistics from the fully turbulent channel flow showed that vorticity stretching is active in the near-wall region, with a peak in the viscous sublayer ($y^+ \approx 6.5$) and dominates over vorticity tilting. Further out in the outer region of the flow where the turbulence is more isotropic, the enstrophy produced solely by stretching compared to the total enstrophy production attains a constant value of $\sim 1/3$. In summary, the proposed diagnostic applied to a turbulent flow finds regions where high-speed streaks create drag or streak instabilities are present (both sinuous and varicose). As opposed to vortices which are simply convected away from the 'active' region of the flow as soon as they are created and hence are generally seen to be located far from the wall, where the turbulent production is low; high concentrations of vorticity stretching are mainly found in regions where growing instabilities are present and hence dynamically important.

ACKNOWLEDGEMENTS

The NORDITA Workshop on Turbulent Boundary Layers 2010 is acknowledged for providing a forum for the present collaboration and thus making this project possible.

REFERENCES

Chevalier, M., Schlatter, P., Lundbladh, A. & Henningson, D. S. 2007 A Pseudo-Spectral Solver for Incompressible Boundary Layer Flows. *Tech. Rep.* TRITA-MEK 2007:07. Royal Institute of Technology (KTH), Dept. of Mechanics, Stockholm.

Gilbert, N. & Kleiser, L. 1990 Near-wall phenomena in transition to turbulence. In *Near-Wall Turbulence* (ed. S.J. Kline & N.H. Afgan), pp. 7–27. 1988 Zoran Zarić Memorial Conference, New York, USA.

Hamilton, J. M., Kim, J. & Waleffe, F. 1995 Regeneration mechanisms of near-wall turbulence structures. *J. Fluid Mech.* **287**, 317–348.

Jeong, J. & Hussain, F. 1995 On the identification of a vortex. *J. Fluid Mech.* **285**, 69–94.

Jeong, J., Hussain, F., Schoppa, W. & Kim, J. 1997 Coherent structures near the wall in a turbulent channel flow. *J. Fluid Mech.* **332**, 185–214.

Jiménez, J. & Moin, P. 1991 The minimal flow unit in near-wall turbulence. *J. Fluid Mech.* **225**, 213–240.

Jiménez, J. & Pinelli, A. 1999 The autonomous cycle of near-wall turbulence. *J. Fluid Mech.* **389**, 335–359.

Jones, L.E., Sandberg, R.D. & Sandham, N.D. 2009 Local and global stability of airfoil flows at low reynolds number. In *IUTAM Seventh IUTAM Symposium on Laminar-Turbulent Transition* (ed. P. Schlatter & D. S. Henningson). Springer-Verlag.

Klebanoff, P. S., Tidstrom, K. D. & Sargent, L. M. 1962 The three-dimensional nature of boundary-layer instability. *J. Fluid Mech.* **12**, 1–34.

Kline, S. J., Reynolds, W. C., Schraub, F. A. & Runstadler, P. W. 1967 The structure of turbulent boundary layers. *J. Fluid Mech.* **30** (04), 741–773.

Landahl, M. T. 1980 A note on an algebraic instability of inviscid parallel shear flow. *J. Fluid Mech.* **98** (part 2), 243–251.

Madré, T. K. 2011 Turbulence transition in the asymptotic suction boundary layer. Diplomarbeit, Philipps-Universität, Marburg, Germany.

Moser, R. D., Kim, J. & Mansour, N. 1999 Direct numerical simulation of turbulent channel flow up to $\mathrm{Re}_\tau = 590$. *Phys. Fluids* **11** (4), 943–945.

Nomura, K.K. & Post, G.K. 1998 The structure and dynamics of vorticity and rate of strain in incompressible homogeneous turbulence. *J. Fluid Mech.* **377**, 65–97.

Sandham, N. D. & Kleiser, L. 1992 The late stages of transition to turbulence in channel flow. *J. Fluid Mech.* **245**, 319–348.

Schneider, T. M., Eckhardt, B. & Yorke, J. A. 2007 Turbulence transition and the edge of chaos in pipe flow. *Phys. Rev. Lett.* **99** (3), 034502.

Schoppa, W. & Hussain, F. 2002 Coherent structure generation in near-wall turbulence. *J. Fluid Mech.* **453**, 57–108.

She, Z.-S., Jackson, E. & Orszag, S. A. 1991 Structure and dynamics of homogeneous turbulence: Models and simulations. *Proc. R. Soc. Lond.* **434** (1890), pp. 101–124.

Smith, C. R. & Metzler, S. P. 1983 The characteristics of low-speed streaks in the near-wall region of a turbulent boundary layer. *J. Fluid Mech.* **129**, 27–54.

Waleffe, F. 1997 On a self-sustaining process in shear flows. *Physics of Fluids* **9** (4), 883–900.